Thermotropic and Lyotropic Behavior of a PEO−PPO−PEO Block Copolymer

Birgitta Svensson*,† and Ulf Olsson‡

Institute for Surface Chemistry, P.O. Box 5607, Se-114 86 Stockholm, Sweden, and Physical Chemistry 1, Center for Chemistry and Chemical Engineering, Lund University, P.O. Box 124, SE-221 00 Lund, Sweden

Received December 27, 1999; Revised Manuscript Received July 28, 2000

ABSTRACT: The phase behavior of the $(EO)_{19}(PO)_{43}(EO)_{19}$/*p*-xylene system (where EO is ethylene oxide and PO is propylene oxide) with temperature is discussed. In this block copolymer the end blocks are crystallizable, and the middle block is noncrystallizable. Several techniques were used to delineate the phase boundaries (SAXS, WAXS, ^{1}H NMR, ^{2}H NMR, and DSC). An anisotropic region with a lamellar structure with semicrystalline PEO domains and amorphous PPO domains is formed at low temperatures and high copolymer concentrations. The lamellar structure has a one-dimensional swelling with increasing *p*-xylene concentration. The driving force for forming the anisotropic region is that the PEO crystallize at low temperatures. The amount of crystallinity in the system and the interfacial area per PEO block in the ordered region depend on the temperature and the sample composition. At high temperatures and low copolymer concentrations the system contains an isotopic solution phase.

1. Introduction

Block copolymers with one crystallizable block and one noncrystallizable block have been studied a few decades. One example of such a copolymer is a block copolymer of poly(ethylene oxide) and poly(propylene oxide), where poly(ethylene oxide) (PEO) can be partly crystalline (semicrystalline) at ambient temperatures, while the poly(propylene oxide) (PPO) is amorphous at temperatures above its glass transition temperature, T_g, which is 207 K.[1] (The melting temperature, T_m, is always greater than the T_g for partly crystalline materials, and the difference is a maximum for homopolymers.) Several papers have been reported on the melting behavior of block copolymers with semicrystalline PEO blocks and different amorphous blocks. The melting temperature of the crystalline structure depends on the block molecular weight, the copolymer architecture, and the solvent conditions.[2−9] The PEO/PPO block copolymers as well as the other semicrystalline block copolymers have very interesting characteristics with varied temperature and upon addition of solvent, and these characteristics are therefore important to understand.

The poly(ethylene oxide) homopolymer is crystalline at ambient temperatures if the molecular weight is larger than approximately 1000.[10] The melting procedure of the PEO homopolymer depends on the polymer molecular weight. At low molecular weight (<4000), the polymer has an extended conformation, although several degrees of lamellar chain folding may exist at larger molecular weight during the melting procedure.[11] The melting points of copolymers with PEO blocks are lower than these of PEO homopolymers having the same number of ethylene oxide units.[2,3,10] The degree of crystallinity is also significantly lower than that of the homologous homopolymer.[12,13] A lamellar structure is the most common mesostructure if one block is partly crystalline, but hexagonal structures have been reported for PDMS/PEO block copolymers.[13]

* To whom correspondence should be addressed. E-mail Birgitta.Svensson@surfchem.kth.se.
† Institute for Surface Chemistry.
‡ Lund University.

Studies of semicrystalline PEO/PPO copolymers in the absence of solvent show that the polymeric system forms well-ordered lamellar domains. Experimental results show that the crystalline structure of the PEO in the semicrystalline aggregates depends on the length of the PEO chain, the length of the amorphous PPO block, and the copolymer architecture.[2,3,5,7,10,12] Theoretical work by Whitmore et al.[14] shows that chain folding leads to a less dense packing of the amorphous blocks. This increases the entropy but gives an increased interfacial area per PEO block, thus leading to increased enthalpy of the system. These opposing forces lead to different numbers of chain folding depending on the molecular weight and the copolymer architecture. Some other studies on the structure of PEO/PBO block copolymers have been reported.[15−18]

PEO/PPO block copolymers and PEO/PBO block copolymers in selective solvents form micelles and various liquid crystalline phases depending on the sample compositions (see e.g. refs 19−23 and references therein). However, at high copolymer concentration the semicrystalline structure of the copolymer may remain. Mortensen et al. investigated the structure and phase behavior of PEO/PPO block copolymers without solvent and in aqueous solutions.[8,9] The structure of the $(EO)_{25}(PO)_{40}(EO)_{25}$ triblock copolymer (trade name P85; BASF) at low temperature and with no water present is lamellar with highly stretched copolymer chains. The crystalline PEO domain can be swollen with a small amount of water (≈10 wt %) and still maintain its crystalline structure. The lamellar structure remains up to a temperature of 40 °C, where it melts and forms an unordered solution phase.[9] This behavior has also been observed for the copolymer $(EO)_{43}(PO)_{16}(EO)_{43}$ (trade name F38; BASF) which melts at a temperature of approximately 45 °C.[24] Some studies on other semicrystalline copolymers in water or oil solutions have also been reported.[4,6,25−27]

Here we have studied the $(EO)_{19}(PO)_{43}(EO)_{19}$/*p*-xylene system. This report is organized as follows. After the Experimental Section, the determination of the phase behavior is discussed, and the amount of crystallinity

10.1021/ma992146s CCC: $19.00
Published on Web 09/09/2000

is estimated. Several techniques, such as small and wide-angle X-ray scattering (SAXS and WAXS), ^{1}H and ^{2}H NMR, and DSC, are used to characterize the crystalline phase and to delineate the phase boundaries.

2. Material and Method

Materials and Sample Preparation. The poly(ethylene oxide) (PEO)/poly(propylene oxide) (PPO) copolymer with the trade name Pluronic P84 was obtained as a gift from BASF Corp., New Jersey. According to the manufacturer, the copolymer contains 40 wt % PEO and has the density 1.05 g/mL at 25 °C. The molecular weight is 4200. The resulting composition is $(EO)_{19}(PO)_{43}(EO)_{19}$. The molar volume of the copolymer (v_p) equals 6700 Å^3, calculated from the copolymer density and molecular weight. *p*-Xylene (1,4-dimethylbenzene) of purity >99.0% was obtained from Fluka Chemie AG, Buchs, Switzerland, and deuterated *p*-xylene ($C_6D_4(CD_3)_2$, >99.00 at. % ^{2}H) was purchased from Dr. Glaser AG, Basel, Switzerland. A poly(ethylene oxide) sample with molecular weight 1000 ± 50 ($(EO)_{23}$) was also used. All chemicals were used without further purification.

We note that the copolymer used is a commercial product, which is polydisperse and possibly also contains impurities. Wu et al. found a value of 1.1 for the ratio M_w/M_n of $(EO)_{13}$-$(PO)_{30}(EO)_{13}$, where M_w and M_n are the weight-averaged and number-averaged molecular weight, respectively.[28] In related copolymers a minor fraction of water insoluble impurity has been reported.[29−31]

Determination of the Phase Boundaries. The samples were prepared individually by weighing appropriate amounts of copolymer and *p*-xylene into 5 mm (i.d.) glass tubes which were flame-sealed immediately. The sample tubes were centrifuged at 25 °C for a period of several days, repeatingly alternating the direction of the tubes. The samples were then left at a given temperature in a temperature-controlled water bath for at least 6 h (longer times for the low temperatures) to attain equilibrium. The samples were examined for flow characteristics and birefringence by inspection between crossed polarizers at each temperature.

Rheological Experiments. Oscillatory shear measurements were carried out on two concentrations of the $(EO)_{19}$-$(PO)_{43}(EO)_{19}$/*p*-xylene system (80 and 90 wt % copolymer) using a Physica UDS 200 rheometer equipped with an automatic gap setting and a cone and plate geometry (25 or 50 mm depending on the viscosity). The temperature was controlled within 0.1 °C with a Peltier system, and the samples were protected from *p*-xylene evaporation by using a solvent trap during the measurement. At each temperature the sample was checked to be within the linear viscoelastic region where the dynamic storage modulus, G', and the loss modulus, G'', are independent of the applied stress. Oscillatory measurements in the frequency range 0.1−100 Hz were then recorded.

Differential Scanning Calorimetry (DSC). The thermal properties of the copolymer and the solution mixtures were analyzed with a Mettler TC 10A/TC15 system. Analyses were made on samples (11−17 mg) contained in sealed aluminum pans. The measurement started at 25 °C, and then the sample was cooled to −20 °C and then heated to 50 or 60 °C. The temperature scan rate was 10 °C/min. One sample (100% $(EO)_{19}(PO)_{43}(EO)_{19}$) was also scanned at 1 °C/min. Essentially no difference compared to the higher scan rate could be observed.

Structural Characterization Using Small-Angle X-ray Scattering (SAXS) and Wide-Angle X-ray Scattering (WAXS). The samples were prepared individually by weighing appropriate amounts of copolymer and *p*-xylene into sample tubes. The SAXS/WAXS measurements were performed on a Kratky compact small-angle system and a wide-angle system equipped with position-sensitive detectors (OED 50M from MBraun, Austria) containing 1024 channels of width 53.6 μm. Cu Kα radiation of wavelength 1.542 Å was provided by a Seifert ID-300 X-ray generator, operating at 50 kV and 40 mA. To minimize the scattering from air, the camera volume was kept under vacuum during the measurements. A Peltier element controlled the temperature within ±0.1 °C. The sample holder was a 1 mm quartz capillary, and the samples were filled into the capillary by using a syringe. A 10 μm thick Ni filter was used to remove the K_β radiation, and a 1.5 mm W filter was used to protect the detector from the primary beam. The sample-to-detector distance was 277 mm. The peak positions were evaluated from the slit-smeared SAXS data.

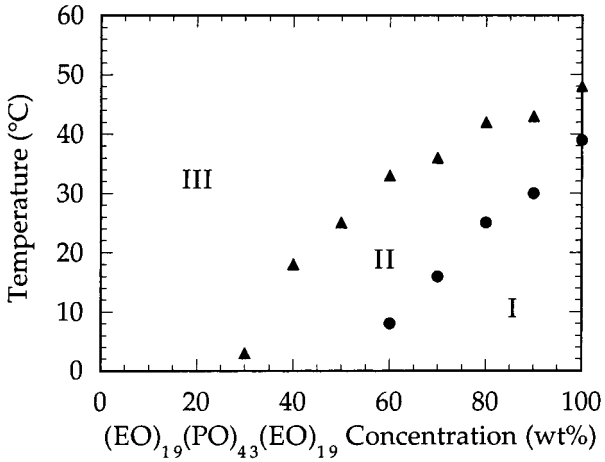

Figure 1. Diagram of the $(EO)_{19}(PO)_{43}(EO)_{19}$/*p*-xylene system. The symbols represent the following visual observations: temperature where the sample flows (●) and temperature where the sample becomes isotropic (▲). Three regions are indicated: region I, an anisotropic region, region II, a two-phase region, and region III, an isotropic solution region.

^{1}H NMR and ^{2}H NMR. The phase equilibrium was also investigated by recording ^{1}H NMR and ^{2}H NMR spectra. The samples were prepared individually by weighing appropriate amounts of copolymer and *p*-xylene-d_{10} into 5 mm NMR tubes (with approximately 25 mm sample solution) which were flame-sealed immediately. The NMR experiments were performed on a Bruker CXP 200 spectrometer at a resonance frequency of 30.7 MHz. The sample was temperature controlled by passing air through the sample holder.

3. Results

Visual Observations. The diagram of the $(EO)_{19}$-$(PO)_{43}(EO)_{19}$/*p*-xylene system is presented in Figure 1, plotted as temperature versus the copolymer weight fraction. The diagram consists of three different regions, which we have denoted I, II, and III. Samples in region I are very viscous, slightly turbid, and optically birefringent. When samples in region I are slowly heated, they suddenly begin to flow at a rather well-defined temperature. In region II, the samples flow. However, when viewed between crossed polarizers, they are still slightly turbid and show optical birefringence. Finally, if the samples are heated further, the turbidity and optical birefringence disappear completely, and the samples become transparent isotropic liquids. This isotropic liquid region is denoted III. If samples in region II are left to stand, a macroscopic phase separation is observed where a low-viscosity liquid phase coexists with a viscous anisotropic phase. Because of the increase in the overall viscosity, the time it takes to achieve macroscopic phase separation increases strongly with the copolymer concentration. No macroscopic phase separation could be detected in region II within a week, above 80 wt % copolymer. Nevertheless, phase separation was achieved upon centrifugation.

We note here that the solvent-free sample (100% $(EO)_{19}(PO)_{43}(EO)_{19}$) also shows a two-phase region. This is most likely a consequence of impurities in the copolymer, which is a commercial product.

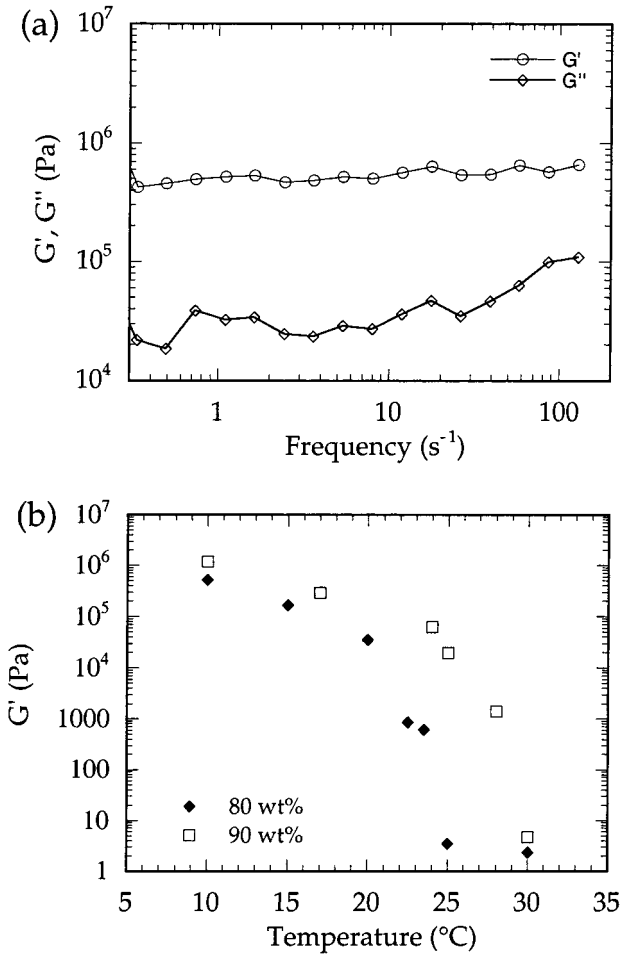

Figure 2. (a) Frequency sweep of the elastic storage modulus G' (○) and the loss modulus G'' (◇) for a sample containing 80 wt % $(EO)_{19}(PO)_{43}(EO)_{19}$ at 10 °C. (b) The temperature dependence of G' recorded at 10 Hz for two samples: 90 wt % $(EO)_{19}(PO)_{43}(EO)_{19}$ and 10 wt % *p*-xylene (□); 80 wt % $(EO)_{19}(PO)_{43}(EO)_{19}$ and 20 wt % *p*-xylene (◆).

Rheology. The dramatic change in viscosity, when passing from region I to region II, was confirmed by oscillatory rheological measurements. Deep into the anisotropic phase (region I) the samples are elastic. Here, the storage (G') and loss (G'') moduli are essentially frequency-independent within the explored frequency range (0.1−100 Hz), where $G' \gg G''$. As a typical example, Figure 2a shows a frequency sweep of G' and G'' for a sample containing 80 wt % $(EO)_{19}(PO)_{43}(EO)_{19}$ at 10 °C. Note that the value of G' is very high, on the order of MPa. In other words, the sample is very "stiff". Figure 2b shows the temperature dependence of G' recorded at 10 Hz for two samples, 80 and 90 wt % $(EO)_{19}(PO)_{43}(EO)_{19}$ in *p*-xylene, respectively. At 10 °C the G' moduli are very high but drop many orders of magnitude within a few degrees. At a temperature above 25 °C for the 80 wt % sample and 30 °C for the 90 wt % sample, the samples flow. The drop in G' in the vicinity of the transition shows that the transformation from "stiff" to fluid is sharp.

Differential Scanning Calorimetry (DSC). To characterize the phase transition (order−disorder) from the anisotropic to the isotropic phase further, we performed differential scanning calorimetry (DSC) measurements for a number of samples, crossing the phase transition. In Figure 3 we show the melting behavior of three concentrations: 100, 90, and 80 wt % $(EO)_{19}(PO)_{43}(EO)_{19}$ in *p*-xylene. Two peaks in the DSC curves are observed for all samples. The high-temperature peak is related to the anisotropic to liquid transition, and the broad low-temperature peak corresponds to a process occurring within the semicrystalline region (region I).

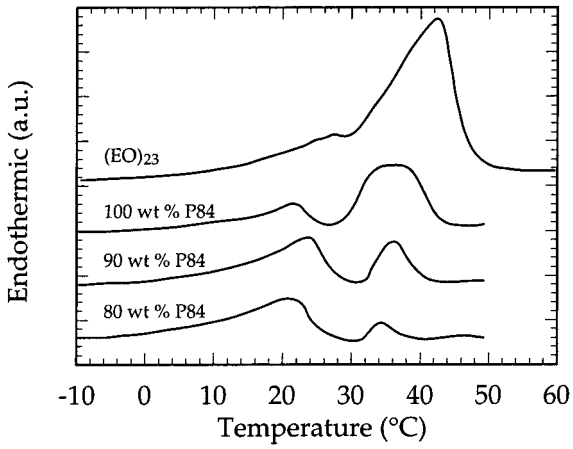

Figure 3. DSC melting curves at heating rate 10 °C/min. The sample compositions from the top are (1) 100% $(EO)_{23}$, (2) 100% $(EO)_{19}(PO)_{43}(EO)_{19}$, (3) 90 wt % $(EO)_{19}(PO)_{43}(EO)_{19}$ and 10 wt % *p*-xylene, and (4) 80 wt % $(EO)_{19}(PO)_{43}(EO)_{19}$ and 20 wt % *p*-xylene.

For comparative purposes, we also show a DSC scan of a sample containing the PEO homopolymer $(EO)_{23}$ in Figure 3. Thus, it appears that the formation of the anisotropic phase at lower temperatures and higher copolymer concentrations is related to the crystallization of the PEO blocks. The DSC curves do not allow for measurement of the enthalpy of fusion and thereby to assessment of the extent of crystallinity. This is due to the crystal size polydispersity, which is dependent on the annealing temperature, and the polydispersity of the copolymer. Below we will investigate the crystallinity of the anisotropic phase in more detail using small- and wide-angle X-ray scattering and ^1H and ^2H NMR.

Wide-Angle X-ray Scattering (WAXS). Studies by wide-angle X-ray scattering yield information about the crystal structure and degree of crystallinity, as the technique probes structures on the length scale 2−5 Å. The WAXS diffraction patterns at temperatures between 5 and 40 °C for two concentrations of copolymer $(EO)_{19}(PO)_{43}(EO)_{19}$, 100 and 70 wt %, are shown in Figure 4, parts a and b. For comparison, the scattering from the $(EO)_{23}$ homopolymer at 5 °C is shown in Figure 4c. (For indexation of the peaks, see ref 33.) The block copolymer diffraction patterns show the same wide angle peaks as the homopolymer, and thus the Bragg peaks from the copolymer can be indexed to a crystal structure of the poly(ethylene oxide). Upon increased temperature, the peak intensity decreases, indicating a gradual melting of the crystalline order. The peak intensity from the pure (solvent-free) block copolymer vanishes at about 35 °C. Increased *p*-xylene content decreases the melting temperature.

^1H NMR. Polymer chain mobility is different in amorphous and crystalline regions. The shapes of the ^1H NMR spectra are sensitive to this mobility, and therefore we used the technique to study the amount of crystallinity of the $(EO)_{19}(PO)_{43}(EO)_{19}$/*p*-xylene-$d_{10}$ system with temperature. The ^1H NMR spectra are characterized by the protons in the copolymer. The ^1H NMR spectra recorded contain in essence two signals: one from overlapping [−CH_2−] and [−CH−] bands and

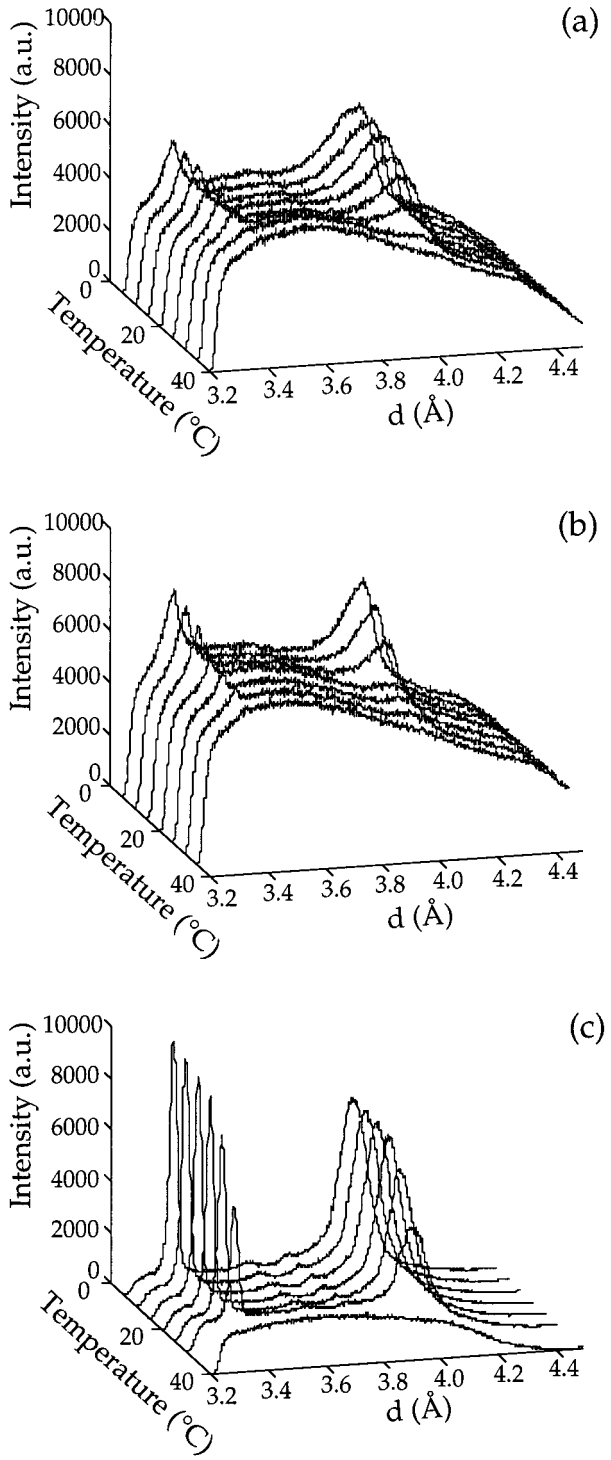

Figure 4. WAXS diffraction patterns with varied temperature between 5 and 40 °C: (a) copolymer $(EO)_{19}(PO)_{43}(EO)_{19}$, (b) sample composition 70 wt % $(EO)_{19}(PO)_{43}(EO)_{19}$ and 30 wt % *p*-xylene, and (c) homopolymer $(EO)_{23}$.

one from $[-CH_3-]$. The $[-CH_2-] + [-CH-]$ signal is broad at low temperatures and becomes progressively resolved at higher temperatures. Figure 5a shows a selective frequency region of the ^1H NMR spectra for the 90 wt % copolymer and 10 wt % *p*-xylene-d_{10} sample.

It is interesting to analyze the area under the NMR bands since we expect proton signal from crystalline domains to be very broad. With the proviso that the exchange rates are slow enough, this system can be analyzed by recording a superposition of each spectrum of the exchange of EO segment between the crystalline

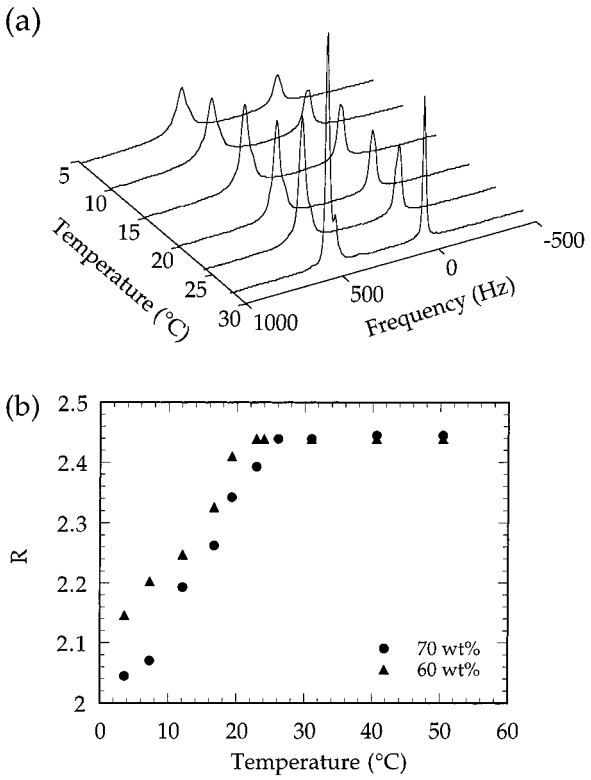

Figure 5. (a) ^1H NMR spectra of the 90 wt % $(EO)_{19}(PO)_{43}(EO)_{19}$ and 10 wt % *p*-xylene-d_{10} sample at different temperatures. (b) The area ratio $[-CH_2-] + [-CH-]$ signal to the $[-CH_3-]$ signal, *R*, as a function of temperature. The sample compositions are 70 wt % $(EO)_{19}(PO)_{43}(EO)_{19}$ and 30 wt % *p*-xylene-d_{10} (●) and 60 wt % $(EO)_{19}(PO)_{43}(EO)_{19}$ and 40 wt % *p*-xylene-d_{10} (▲).

and noncrystalline parts, respectively. However, the resonance from crystalline parts will effectively not contribute to the measured intensity. The area ratio, *R*, between the $[-CH_2-] + [-CH-]$ and $[-CH_3-]$ does indeed depend on the temperature. *R* is plotted as a function of the temperature for two copolymer concentrations, 60 and 70 wt %, respectively, in Figure 5b. At higher copolymer concentrations the two signals overlap too much at lower temperatures to allow for an accurate area analysis. At higher temperatures, in the liquid phase, where all protons contribute, we find $R = 2.44$ and no temperature dependence. This value of *R* is close to, but slightly larger than, the value 2.19, which is expected for our block copolymer composition $(EO)_{19}(PO)_{43}(EO)_{19}$. ($R = 2.44$ is consistent with a copolymer having slightly higher EO content.) At lower temperatures, the *R* ratio decreases, indicating that the crystallinity increases. The amount of crystalline material, *A*, in the sample can be calculated from

$$A = 1 - \frac{R}{2.44} \tag{1}$$

Figure 6 shows the amount of crystallinity as a function of temperature, for the compositions 60 and 70 wt % $(EO)_{19}(PO)_{43}(EO)_{19}$ in *p*-xylene-d_{10}. At the lowest temperature the amount of crystalline material corresponds approximately to 17% of the EO content for the 70 wt % sample. Increased temperature leads to reduced amount of crystalline material. Decreased copolymer concentration is also leading to lowered amount of crystalline material as well as crystal melting temperature.

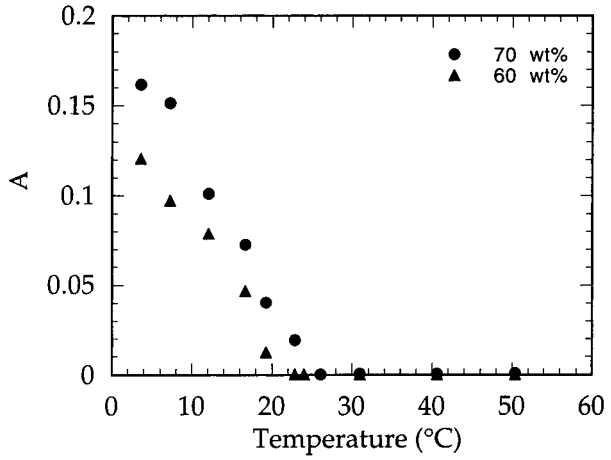

Figure 6. Amount of crystallinity, *A*, determined by ^{1}H NMR as a function of temperature. The sample compositions are 70 wt % $(EO)_{19}(PO)_{43}(EO)_{19}$ and 30 wt % *p*-xylene-d_{10} (●) and 60 wt % $(EO)_{19}(PO)_{43}(EO)_{19}$ and 40 wt % *p*-xylene-d_{10} (▲).

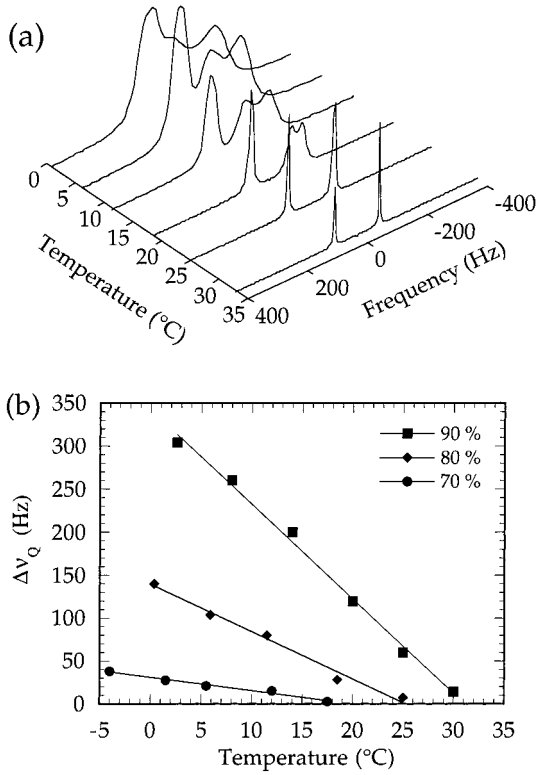

Figure 7. (a) ^{2}H NMR spectra from the 80 wt % $(EO)_{19}(PO)_{43}(EO)_{19}$ and 20 wt % *p*-xylene-d_{10} sample at different temperatures. (b) The dependence of the quadropolar splitting with temperature. The samples are shown with the following symbols: 90 wt % $(EO)_{19}(PO)_{43}(EO)_{19}$ and 10 wt % *p*-xylene-d_{10} (■); 80 wt % $(EO)_{19}(PO)_{43}(EO)_{19}$ and 20 wt % *p*-xylene-d_{10} (◆); 70 wt % $(EO)_{19}(PO)_{43}(EO)_{19}$ and 30 wt % *p*-xylene-d_{10} (●).

^{2}H NMR. ^{2}H NMR, using e.g. a deuterium-labeled solvent, is a useful technique for probing anisotropy.[32] The ^{2}H nucleus has a spin quantum number $I = 1$ and a strong quadrupolar moment. In an isotropic environment, the quadrupolar interaction can be completely averaged to zero, and the spectrum consists of a singlet. On the other hand, in an anisotropic environment, the quadrupolar interaction is only partly averaged, resulting in a splitting into two peaks, a so-called quadropolar splitting. Here we have used deuterated *p*-xylene, which we expect to be primarily located in PPO-rich domains in the case of a structural segregation into "polar" PEO domains and "apolar" PPO domains.

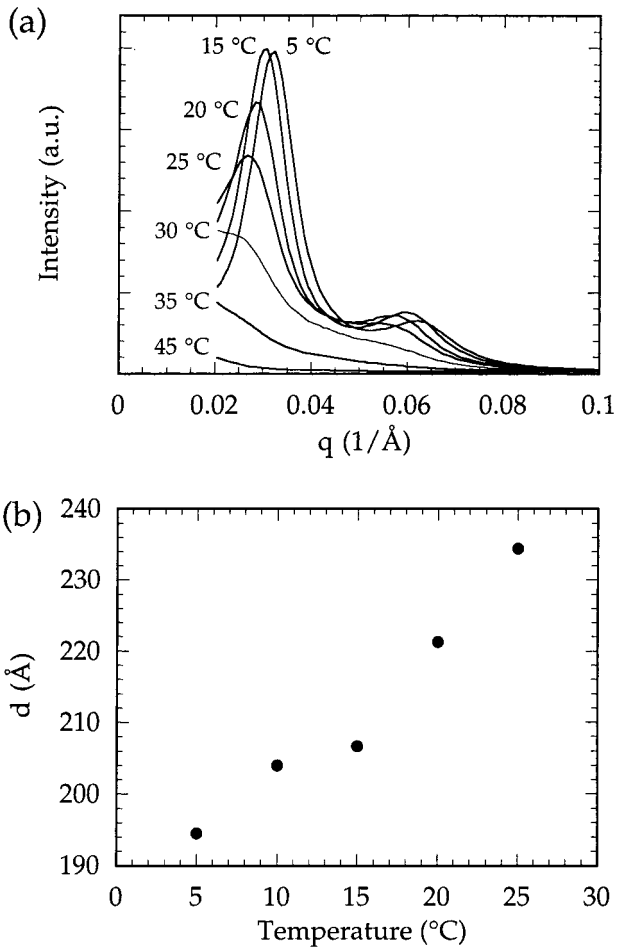

Figure 8. (a) SAXS diffraction patterns of the $(EO)_{19}(PO)_{43}(EO)_{19}$ copolymer between 5 and 45 °C. The temperature is given next to each spectrum. (b) The temperature dependence of the lamellar periodicity, *d*, for the $(EO)_{19}(PO)_{43}(EO)_{19}$ copolymer.

^{2}H NMR spectra were recorded for samples with compositions 70−90 wt % $(EO)_{19}(PO)_{43}(EO)_{19}$ in *p*-xylene-d_{10}. A selective frequency region of the ^{2}H NMR spectra of the 80 wt % $(EO)_{19}(PO)_{43}(EO)_{19}$ sample at temperatures from 0.4 to 33.1 °C is shown in Figure 7a. The samples were equilibrated for at least 30 min at each temperature. To be sure that the equilibrium structure was reached at each temperature, the quadropolar splitting was measured in both melting the structure by increasing the temperature and then crystallizing the structure by decreasing the temperature. Two ^{2}H NMR signals are given from fully deuterated *p*-xylene: one from the aromatic deuterons and one from the methyl groups. The aromatic deuterons have a low order parameter, and quadropolar splittings are sometimes not resolved. Therefore, we focus on the larger splittings recorded from deuterons in the methyl group.

The resulting quadropolar splitting, $\Delta\nu$, of the [$-CD_3-$] peak for all samples studied are shown in Figure 7b. No two-phase regions with an anisotropic signal and an isotropic signal coexisting were observed. In the region I the observed $\Delta\nu$ becomes progressively smaller with increasing temperature, and $\Delta\nu \approx 0$ at the border between region I and II. The $\Delta\nu$ becomes also relatively smaller at decreased copolymer concentration.

Small-Angle X-ray Scattering (SAXS). In Figure 8a, we present the small-angle diffraction patterns

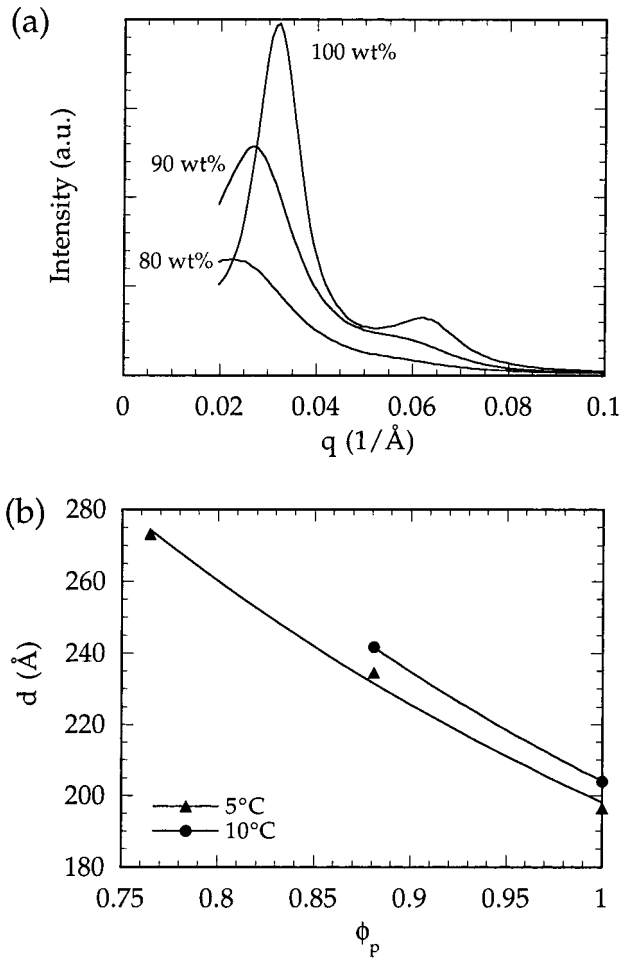

Figure 9. (a) SAXS diffraction patterns of the $(EO)_{19}(PO)_{43}(EO)_{19}$/*p*-xylene system at 5 °C. The copolymer composition is given next to the respectively spectrum. (b) The lamellar periodicity, *d*, dependence on $(EO)_{19}(PO)_{43}(EO)_{19}$ volume fraction, ϕ_p, at two temperatures: 5 °C (▲) and 10 °C (●).

obtained at different temperatures for the copolymer $(EO)_{19}(PO)_{43}(EO)_{19}$. The diffraction patterns at temperatures <35 °C (i.e., from region I) show two peaks that are related as 1:2. This is consistent with a one-dimensional lamellar structure. With increasing temperature, the peaks move to lower *q*, while at the same time the overall scattered intensity decreases. For a lamellar structure, the repeat distance is given by

$$d = \frac{2\pi}{q_1} \tag{2}$$

where q_1 is the scattering vector magnitude of the first reflection. The lamellar periodicity, *d*, increases significantly with increasing temperature, which is shown in Figure 8b. No peaks are observed in region II and III (temperatures > 40 °C), indicating that there is no (or very weak) segregation between the PEO and PPO.

Upon addition of xylene, the peaks also moves to lower *q*, showing that the solvent swells the lamellar structure. The diffraction patterns at 5 °C for copolymer concentration 80, 90, and 100 wt % are shown in Figure 9a. The lamellar periodicity variations with copolymer concentration, at two temperatures (5 and 10 °C), are shown in Figure 9b. The best fit to one-dimensional swelling ($d \sim \phi_p^{-1}$) is included in the figure.

4. Discussion

In the previous section we have presented results from a large variety of techniques, probing the behavior of the $(EO)_{19}(PO)_{43}(EO)_{19}$ copolymer as a function of temperature and upon addition of the apolar solvent *p*-xylene. The $(EO)_{19}(PO)_{43}(EO)_{19}$/*p*-xylene diagram contains two phases in the observed temperature interval, 0−60 °C, separated by a two-phase region. At low copolymer concentrations, an isotropic liquid solution phase is formed at all temperatures. At higher copolymer concentrations, the solution phase remains at higher temperatures, although an anisotropic phase is formed at lower temperatures.

PEO is a crystallizable polymer, and WAXS data obtained from the anisotropic phase show the presence of crystalline PEO. Using SAXS, we find that the long-range periodic structure is lamellar. Apparently, it is the crystallization of PEO, which is the driving force for the formation of the anisotropic phase and the segregation (structuring) into PEO- and PPO-rich domains. However, the degree of crystallinity is strongly temperature-dependent in the investigated temperature interval.

DSC measurements show two melting processes which are related to the melting of the crystal structure of the PEO. Concerning the progressive melting of crystalline PEO domains, we see strong correlation between the different experimental techniques. The progress melting is seen as decreased WAXS peak intensity and recovering of EO proton intensity in the

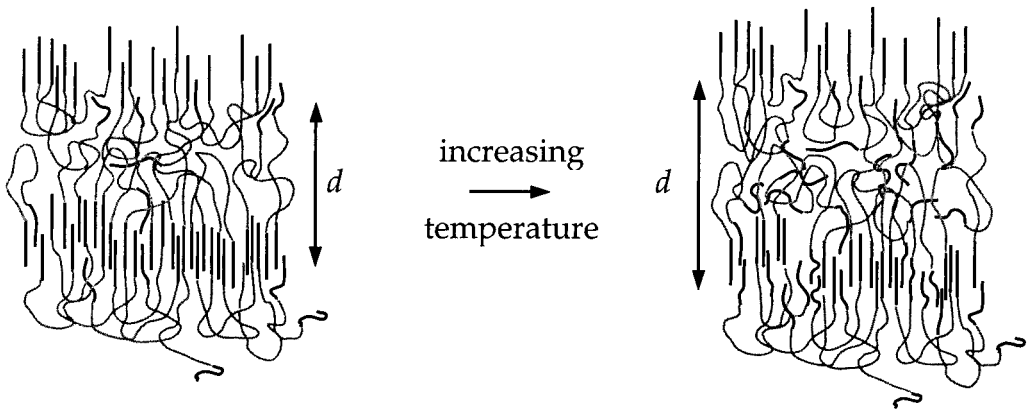

Figure 10. Schematic drawing of the anisotropic lamellar phase in region I in Figure 1 upon increased temperature. The PPO block of the copolymer is depicted in gray, and the PEO is depicted in black. The repeated lamellar distance, *d*, is indicated in the figure.

^{1}H NMR spectrum. The crystalline fraction is of the order of 20% at 5 °C, if the ^{1}H NMR data are analyzed in terms of a two-state model. We note here that the amount of crystallinity is low, which most likely depends on the low molecular weight of the PEO. The lower crystallinity and lower melting points for blocks compared to homopolymers of the same molecular weight are generally observed and are related to increased fluctuations in the vicinity of the amorphous block.[10]

In correlation with the progressive melting, we also see that the lamellar *d* spacing increases and the scattered intensity decreases upon increased temperature (SAXS). The *d* spacing is much larger than what is found in the L_α (liquid crystalline lamellar) phase of the ternary $(EO)_{19}(PO)_{43}(EO)_{19}/D_2O$/*p*-xylene system at the same polymer concentration.[33] Since the area of the PEO/PPO interface becomes smaller for crystalline PEO, a larger *d* spacing is expected. However, the observed crystallinity is low; consequently, the large difference in *d* spacing, compared to what is found in the L_α phase, is probably due to that not all PEO is aggregated into the PEO domains contributing to the lamellar structure. Hence, the PEO concentration in the PPO domain increases with increasing temperature leading to (i) increased *d* spacing due to a reduced lamellar interfacial area and (ii) decreased scattering intensity due to reduced scattering length density difference between PEO and PPO domains. In other words, the segregation between the PEO and PPO decreases with increasing temperature due to the lowered amount of crystalline PEO. The variation with temperature is illustrated in Figure 10. We note here that since the melted PEO block is less stretched and has a larger interfacial area compared to the crystalline case, we would expect the gradual melting to lead to decreased *d* spacing if all the PEO was located in PEO domains.

We have also investigated the phase behavior of the $(EO)_{13}(PO)_{30}(EO)_{13}$/*p*-xylene system between 0 and 60 °C (to be published).[34] The phase behavior is similar to what is observed for the $(EO)_{19}(PO)_{43}(EO)_{19}$/*p*-xylene system studied here. Hence, the thermal phase behavior observed in this work seems general for PEO/PPO block copolymers in selective solvents for the PPO block.

5. Conclusion

The segregation between the polar and the apolar domain in PEO−PPO−PEO systems depends on the amount of solvent added. In *p*-xylene in the melted condition, adding a small amount of water can induce micelle formation.[28,35] Here, we have demonstrated that lowering the temperature, where the PEO blocks crystallize, also induces structure. We have also shown that the degree of crystallinity decreases gradually with increasing temperature and increasing amount of *p*-xylene.

Acknowledgment. B.S. acknowledges financial support from the Center of Competence for Amphiphilic Polymers from Renewable Resources, Lund University, Sweden. The acquisition of the SAXS apparatus was funded by the Swedish Council for Planning and Coordination of Research (FRN). Åsa Halldén is kindly acknowledged for helping us with the DSC measurements.

References and Notes

(1) Morales, E.; Salmerón, M.; Acosta, J. L. *J. Polym. Sci., Part B* **1996**, *34*, 2715.
(2) Booth, C.; Pickles, C. J. *J. Polym. Sci., Polym. Phys. Ed.* **1973**, *11*, 249.
(3) Booth, C.; Dodgson, D. V. *J. Polym. Sci., Polym. Phys. Ed.* **1973**, *11*, 265.
(4) Gervais, M.; Gallot, B. *Makromol. Chem.* **1973**, *171*, 157.
(5) Ashman, P.-C.; Booth, C. *Polymer* **1975**, *16*, 889.
(6) Gervais, M.; Gallot, B. *Makromol. Chem.* **1977**, *178*, 1577.
(7) Viras, F.; Luo, Y.-Z.; Viras, K.; Mobbs, R. H.; King, T. A.; Booth, C. *Makromol. Chem.* **1988**, *189*, 459.
(8) Mortensen, K.; Brown, W.; Jørgensen, E. *Macromolecules* **1994**, *27*, 5654.
(9) Mortensen, K.; Brown, W.; Jørgensen, E. *Macromolecules* **1995**, *28*, 1458.
(10) Simek, L.; Petrík, S.; Hadobas, F.; Bohdanecky, M. *Eur. Polym. J.* **1990**, *26*, 371.
(11) Beech, D. R.; Booth, C.; Dodgson, D. V.; Sharpe, R. R.; Waring, J. R. S. *Polymer* **1972**, *13*, 73.
(12) Ashman, P. C.; Booth, C.; Cooper, D. R.; Price, C. *Polymer* **1975**, *16*, 897.
(13) Galin, M.; Mathis, A. *Macromolecules* **1981**, *14*, 677.
(14) Whitmore, M. D.; Noolandi, J. *Macromolecules* **1988**, *21*, 1482.
(15) Nace, V. M.; Whitmarsh, R. H.; Edens, M. W. *J. Am. Oil Chem. Soc.* **1994**, *71*, 777.
(16) Yang, Y.-W.; Tanodekaew, S.; Mai, S.-M.; Booth, C.; Ryan, A. J.; Bras, W.; Viras, K. *Macromolecules* **1995**, *28*, 6029.
(17) Ryan, A. J.; Fairclough, J. P. A.; Hamley, I. W.; Mai, S.-M. M.; Booth, C. *Macromolecules* **1997**, *30*, 1723.
(18) Mai, S.-M.; Fairclough, J. P. A.; Viras, K.; Gorry, P. A.; Hamley, I. W.; Ryan, A. J.; Booth, C. *Macromolecules* **1997**, *30*, 8392.
(19) Wanka, G.; Hoffmann, H.; Ulbricht, W. *Macromolecules* **1994**, *27*, 4145.
(20) Alexandridis, P.; Hatton, T. A. *Colloids Surf. A* **1995**, *96*, 1.
(21) Yang, Y.-W.; Yang, Z.; Zhou, Z.-K.; Attwood, D.; Booth, C. *Macromolecules* **1996**, *29*, 670.
(22) Yu, G.-E.; Yang, Y.-W.; Yang, Z.; Attwood, D.; Booth, C.; Nace, V. M. *Langmuir* **1996**, *12*, 3404.
(23) Svensson, B.; Alexandridis, P.; Olsson, U. *J. Phys. Chem. B* **1998**, *102*, 7541.
(24) Svensson, B.; Olsson, U.; Alexandridis, P. Submitted for publication.
(25) Gervais, M.; Gallot, B. *Makromol. Chem.* **1973**, *174*, 193.
(26) Gervais, M.; Gallot, B. *Makromol. Chem.* **1977**, *178*, 2071.
(27) Mortensen, K.; Talmon, Y.; Gao, B.; Kops, J. *Macromolecules* **1997**, *30*, 6764.
(28) Wu, G.; Zhou, Z.; Chu, B. *Macromolecules* **1993**, *26*, 2117.
(29) Zhou, Z.; Chu, B. *Macromolecules* **1988**, *21*, 2548.
(30) Yu, G.-E.; Altinok, H.; Nixon, S. K.; Booth, C.; Alexandridis, P.; Hatton, T. A. *Eur. Polym. J.* **1997**, *33*, 673.
(31) Kositza, M. J.; Bohne, C.; Alexandridis, P.; Hatton, T. A.; Holzwarth, J. F. *Langmuir* **1999**, *15*, 322.
(32) Khan, A.; Fontell, K.; Lindblom, G.; Lindman, B. *J. Phys. Chem.* **1982**, *86*, 4266.
(33) Alexandridis, P.; Olsson, U.; Lindman, B. *Langmuir* **1998**, *14*, 2627.
(34) Svensson, B. Ternary Block Copolymer Systems − Phase Behaviour and Phase Structure. Ph.D. Thesis, Lund University, Lund, Sweden, 2000.
(35) Alexandridis, P.; Andersson, K. *J. Colloid Interface Sci.* **1997**, *194*, 166.

MA992146S